



**Environmental
Science**
Nano

**Natural Organic Matter Adsorption Conditions Influence
Photocatalytic Reaction Pathways of Phosphate-Treated
Titanium Dioxide Nanoparticles**

Journal:	<i>Environmental Science: Nano</i>
Manuscript ID	EN-ART-05-2021-000433.R1
Article Type:	Paper

SCHOLARONE™
Manuscripts

Environmental Significance Statement

Titanium dioxide (TiO₂) nanoparticles are of interest for photocatalytic water treatment, but natural organic matter (NOM) often inhibits their reactivity. Although phosphate treatment has been proposed to mitigate NOM fouling, this study identifies that differences in NOM adsorption from different water chemistries – deionized water (DIW) and moderately hard water (MHW) – persist even after phosphate treatment. Furthermore, the different NOM layers impart divergent influences on the nanoparticle reactivity: more extensive NOM adsorption from MHW inhibits reactivity by occupying adsorptive sites and modifying the reactive oxygen species profile, whereas a thinner NOM layer adsorbed from DIW promotes reactivity through enhanced hole generation. These mechanistic findings are broadly useful to understand the critical role of surface chemistry on the photocatalytic reactivity of nanomaterials.

1
2
3 **Natural Organic Matter Adsorption Conditions Influence Photocatalytic**
4 **Reaction Pathways of Phosphate-Treated Titanium Dioxide Nanoparticles**
5
6
7
8
9

10
11 Riya A. Mathew,¹ Gang Wu,² Ye Zhang,^{3,4} Sheyda Shakiba,¹ Yan Yao,^{3,4} Ah-Lim Tsai,² and

12
13 Stacey M. Louie^{1*}
14
15
16
17

18 ¹Department of Civil and Environmental Engineering, University of Houston, Houston, TX
19
20 77004
21

22 ²Department of Internal Medicine, McGovern Medical School, University of Texas Health
23
24 Science Center at Houston, Houston, TX 77030
25
26

27 ³Department of Electrical and Computer Engineering, University of Houston, Houston, TX
28
29 77004
30

31 ⁴Texas Center for Superconductivity at the University of Houston, Houston, TX 77204
32
33
34
35

36 *Corresponding author:
37

38 Phone: 713-743-8646
39

40 Fax: 713-743-4260
41

42 Email: slouie@uh.edu
43
44
45
46
47

48 **Submitted to *Environmental Science: Nano***
49
50
51
52
53
54
55
56
57

Abstract

Titanium dioxide (TiO_2) nanoparticles have been widely studied for water treatment applications; however, natural organic matter (NOM) is often reported to hamper the efficiency of the nanoparticles toward the degradation of target pollutants. Phosphate treatment has been proposed as a potentially facile solution to this problem, as phosphate competes for TiO_2 surface sites to diminish the NOM adsorption. However, the potential importance of the conditions of the NOM exposure and the residual NOM remaining after phosphate treatment have not been fully explored. Here, we investigate the reactivity of phosphate-treated TiO_2 nanoparticles with NOM coatings adsorbed from two background water chemistries, deionized water ($\text{TiO}_2\text{-NOM}_{\text{DIW}}$) and moderately hard water ($\text{TiO}_2\text{-NOM}_{\text{MHW}}$). Thorough characterization by size exclusion chromatography revealed that the adsorbed NOM was only partially displaced after phosphate treatment, with a higher adsorbed mass and wider variety of NOM species persisting on $\text{TiO}_2\text{-NOM}_{\text{MHW}}$ compared to $\text{TiO}_2\text{-NOM}_{\text{DIW}}$. Although the remaining adsorbed NOM did not significantly influence the degradation rate of phenol as a model pollutant, remarkably distinct effects were observed in the degradation of catechol as an oxidative byproduct of phenol, with $\text{TiO}_2\text{-NOM}_{\text{MHW}}$ hindering catechol degradation and $\text{TiO}_2\text{-NOM}_{\text{DIW}}$ accelerating catechol degradation. The suppressed reactivity for $\text{TiO}_2\text{-NOM}_{\text{MHW}}$ was attributed to hindrance of the physical adsorption of catechol to the TiO_2 surface by the NOM_{MHW} layer as well as changes in the reactive oxygen species profile as measured by electron paramagnetic resonance (EPR) spectroscopy, whereas the enhanced reactivity for $\text{TiO}_2\text{-NOM}_{\text{DIW}}$ was attributed to higher hole formation, suggesting participation of the NOM_{DIW} layer in electron transfer processes. This research highlights the critical importance of the NOM surface coating in directing the mechanisms for pollutant degradation in photocatalytic nano-enabled water treatment applications.

Introduction

Titanium dioxide (TiO₂) nanoparticles (NPs) have widely been evaluated as photocatalysts for water treatment for their potential to degrade recalcitrant pollutants via the generation of reactive oxygen species (ROS) upon ultraviolet (UV) irradiation.¹ However, the reaction efficiency can be hampered in realistic use conditions, as both background electrolytes and natural organic matter (NOM) in the water can scavenge ROS, form secondary radical species, attenuate light radiation or adsorb to the NP surface to compete with the contaminant of interest for active sites at the NP surface.²⁻¹² Alternatively, NOM can induce enhanced reactivity or photosensitization through excitation to triplet state NOM.^{2, 13-16} Kang et al. distinguished that photoreactivity was enhanced in the presence of low concentrations of NOM but suppressed in high concentrations of NOM.⁶ To counter losses in efficiency, phosphate modification of TiO₂ has been proposed. The adsorption of phosphate can confer colloidal stability through electrostatic repulsion.³ Furthermore, although prior reports vary as to whether the phosphate itself promotes^{17, 18} or inhibits³ ROS generation, Long et al. identified a major benefit of phosphate to mitigate the inhibitory effect of humic acid (HA) through competitive adsorption or displacement of HA from the TiO₂ surface.¹⁸ Under certain conditions (high pH, low HA concentration), a slight enhancement of phenol degradation was also observed and was credited to the changes in the conformation and binding mode of HA by phosphate, leading to increased electron transfer and reduced hole scavenging.¹⁸

Given the importance of the properties of the adsorbed NOM layer in promoting or diminishing the efficiency of the TiO₂ NPs in water treatment, a more thorough investigation is warranted into whether the NOM adsorption conditions impact the potential for phosphate treatment to restore the reactivity of NOM-fouled NPs. NOM adsorption onto TiO₂ is well known

1
2
3 to depend not only on the type of NOM (e.g., fulvic versus humic fractions) and its concentration
4
5 but on the water chemistry, pH, presence of background electrolytes, and ionic strength.^{19, 20} In
6
7 particular, the presence of Ca^{2+} can induce higher adsorption of NOM by cationic bridging to the
8
9 TiO_2 surface or entanglement of the NOM.^{21, 22} Adsorptive fractionation of NOM on TiO_2 can also
10
11 occur, with higher molecular weight species from Suwannee River NOM adsorbing in moderately
12
13 hard water.²³ Higher molecular weight NOM species with higher aromaticity have been reported
14
15 to have the greatest influence on the inhibition of TiO_2 NP photoreactivity.⁷ However, it is
16
17 currently unknown whether the initial adsorption conditions of the NOM, and the subsequent
18
19 differences in the adsorbed mass and adsorptive fractionation of the NOM, will have persistent
20
21 effects on the photoreactivity of the TiO_2 NPs, or whether any differences are eliminated upon
22
23 subsequent phosphate treatment that could displace the adsorbed NOM.
24
25
26
27

28
29 A further research gap remains from prior studies on phosphate-treated TiO_2 NPs that only
30
31 monitored degradation of the “parent” contaminant (e.g., phenol), but did not evaluate the
32
33 formation or degradation of reaction byproducts that may have different reaction pathways. For
34
35 example, phenol oxidizes to form primarily two initial isomers: hydroquinone (HQ) and catechol.
36
37 Although phenol has been reported to show primarily hydroxyl radical mediated degradation,^{17, 24}
38
39 catechol has been reported to participate in hole mediated pathways,¹⁷ and in general, the
40
41 generation or degradation of byproducts can differ based on their selectivity to specific types of
42
43 ROS.²⁵ Therefore, it is currently unclear whether the influences of phosphate and NOM on phenol
44
45 degradation can be generalized to other compounds, including phenol byproducts.
46
47
48

49
50 The objective of this paper is to investigate the mechanisms by which different NOM
51
52 coatings influence the photoreactivity of TiO_2 NPs by probing the photodegradation of phenol and
53
54 its two immediate byproducts, catechol and hydroquinone. Bare TiO_2 NPs are compared to those
55
56
57
58
59
60

1
2
3 coated with NOM in deionized water (DIW) and moderately hard water (MHW), with all NPs
4
5 subsequently undergoing phosphate treatment. The adsorbed layers were thoroughly characterized
6
7 during both the NOM adsorption and phosphate treatment processes using size exclusion
8
9 chromatography (SEC) for adsorbed mass and molecular weight fraction, as well as *in situ* Fourier
10
11 transform infrared (FTIR) spectroscopy for the functional moieties. The myriad potential
12
13 mechanisms for differences in the photoreactivity were then evaluated, including the influence of
14
15 the surface coatings on the physical adsorption of the contaminants to the NP surface, as well as
16
17 the production of holes and different types of ROS, including hydroxyl radical (OH[•]) and singlet
18
19 oxygen (¹O₂), as measured in further experiments using probe compounds and electron
20
21 paramagnetic resonance (EPR) spectroscopy. Overall, this research provides an improved
22
23 mechanistic understanding of the importance of the NOM adsorbed layer properties on the
24
25 reactivity and reaction pathways expressed by phosphate-treated TiO₂ NPs.
26
27
28
29
30
31
32

33 **Materials and methods**

34 *Chemical reagents*

35
36
37 Phenol (Acros Organic, 99.5%, NJ, USA), hydroquinone (Alfa Aesar, 99%, Ward Hill,
38
39 MA, USA) and catechol (Alfa Aesar, 99%, Ward Hill, MA, USA) were used as target compounds.
40
41 Titanium dioxide (TiO₂) NPs (Standard Reference Material 1898) were obtained from the National
42
43 Institute of Standards and Technology (NIST) (Gaithersburg, MD). The TiO₂ NPs are composed
44
45 of 76% anatase with particle size of 19 nm ± 2 nm and 24% rutile with particle size of 37 nm ± 6
46
47 nm.²⁶ Suwannee River NOM (Cat. No. 2R101N) was procured from the International Humic
48
49 Substances Society; the bulk elemental and functional group composition are provided in the
50
51 Supplementary Information (SI), and the molar mass distribution was measured herein. Stock
52
53
54
55
56
57
58
59
60

1
2
3 solutions of NOM were prepared at 1 g/L in deionized water and adjusted to pH \approx 7 using 1 M and
4 0.1 M NaOH. Calcium chloride (CaCl_2) (> 97 %, anhydrous, ACS grade, Sigma-Aldrich) and
5 sodium bicarbonate (NaHCO_3) (> 99.7 %, ACS grade, Sigma-Aldrich) were used to prepare the
6 moderately hard water matrix, and potassium phosphate monobasic anhydrous (KH_2PO_4) (ACS
7 grade, Amresco, Solon, OH) and sodium phosphate dibasic heptahydrate ($\text{Na}_2\text{HPO}_4 \cdot 7\text{H}_2\text{O}$) (ACS
8 grade, Amresco, Solon, OH) for the phosphate buffer. 0.1 M or 1 M HCl (ACS reagent, Sigma-
9 Aldrich) or NaOH (Sigma-Aldrich) were used for pH adjustment.

10
11 Potassium iodide (KI) (Alfa Aesar, 99.9%, Ward Hill, MA, USA) and furfuryl alcohol
12 (FFA) (Sigma Aldrich, 98%) were used as probe compounds for holes and $^1\text{O}_2$, respectively.^{3, 27,}
13 ²⁸ Iodine (0.025 N) and starch indicator (1% (w/v)) (both from VWR International, PA, USA) were
14 used for calibration and as an indicator, respectively, to evaluate KI oxidation. For EPR
15 measurements, BMPO (Enzo Life Science, Farmingdale, NY) was used as a spin trap. For LC
16 measurements, acetic acid (glacial, Macron Fine Chemicals, Radnor, PA) and LC-MS grade water
17 and methanol (OmniSolv, MilliporeSigma, Burlington, MA) were used to prepare the mobile
18 phase.

19 20 21 22 23 24 25 26 27 28 29 30 31 32 33 34 35 36 37 38 39 40 *Preparation of NP stock suspensions*

41
42 TiO_2 stock suspensions (2 g/L) were freshly prepared for each individual experiment in 15
43 mL of DIW using an adapted dispersion protocol:²⁶ 3 mL of DIW was added to 30 mg TiO_2
44 powder, bath sonicated for 30 seconds to form a slurry (Branson CPX1800H, Danbury, CT),
45 followed by the addition of 4.5 mL DIW and probe sonicated for 15 min at an 80% pulse cycle (8
46 s on, 2 s off) (Fisher brand Model 120 Sonic Dismembrator, Fisher Scientific, Hampton, New
47 Hampshire), and finally dilution with 7.5 mL to the desired concentration and volume. The
48
49
50
51
52
53
54
55
56
57
58
59
60

1
2
3 multiple stages of wetting, sonication, and dilution were identified in preliminary experiments to
4 yield reproducible dispersions, where the hydrodynamic size of the NP stocks was verified on each
5 stock preparation using dynamic light scattering (DLS) (Zetasizer Nano ZS, Malvern Instruments,
6 Malvern, United Kingdom) upon diluting the NPs to 0.1 g/L in 1 mM NaCl. The measured z-
7 average and volume-weighted average diameters were 162 ± 7 nm and 119 ± 7 nm, respectively,
8 for 20 independent batches.
9
10
11
12
13
14
15
16
17
18

19 *Preparation and phosphate treatment of NOM-coated and bare TiO₂ NPs*

20
21 The stock NP suspensions were used to prepare NOM-coated TiO₂ NPs (0.5 g/L NPs and
22 0.2 g/L NOM) in two different water matrices – deionized water (DIW) and a simplified
23 moderately hard water (MHW) comprised of 0.85 mM CaCl₂ and 1.2 mM NaHCO₃. The measured
24 pH was ≈ 7 in DIW and ≈ 7.5 in MHW during the adsorption (after diluting the TiO₂ stock
25 suspension and mixing with the pH-adjusted NOM stock), i.e., the pH was near the isoelectric
26 point of 7 for the bare TiO₂.²⁶ All TiO₂ suspensions (bare and coated) were rotated end-over-end
27 at 25 rpm for approximately 20 hours to equilibrate, then centrifuged at 9000 rpm (9418 g) for 15
28 min (Sorvall Legend XTR, Thermo Scientific, Waltham, MA), and the supernatant was removed
29 for TOC and SEC analysis of the unadsorbed NOM. The NPs were then washed twice into 10 mM
30 phosphate buffer (pH 8, 1.4 mM KH₂PO₄ and 8.6 mM Na₂HPO₄) by adding phosphate buffer equal
31 to the volume of supernatant collected, followed by centrifugation and collection of supernatants
32 from each wash for SEC analysis. The hydrodynamic sizes of the uncoated and NOM coated TiO₂
33 suspensions were measured after phosphate treatment and further dilution to 0.1 g/L in the 10 mM
34 phosphate buffer and verified to be similar to that of the stock suspension (see Results and
35
36
37
38
39
40
41
42
43
44
45
46
47
48
49
50
51
52
53
54
55
56
57
58
59
60

1
2
3 Discussion). The zeta potentials were also measured by electrophoretic light scattering (method
4 and results in the SI).
5
6

7
8 To prepare uncoated (bare) TiO₂ NPs, the NP preparation was designed to be as comparable
9
10 to the NOM coating conditions as possible while avoiding any extensive agglomeration that could
11 influence the reactivity. For the DIW condition, the NP stock was diluted to 0.5 g/L in DIW at the
12 “natural” pH of the suspension (pH 5 after dilution). Note that the isoelectric point of the TiO₂ NPs
13 is ≈ 7 ,²⁶ and hence the NPs rapidly agglomerate at pH 7 if NOM is not present to provide colloidal
14 stability. Similarly, an uncoated control could not be prepared in the complete MHW matrix
15 because Ca²⁺ induces rapid formation of agglomerates. However, to investigate the potential
16 influence of HCO₃⁻ adsorption from the MHW, phenol degradation studies were also conducted
17 on bicarbonate-exposed TiO₂ NPs prepared as above in 1.2 mM NaHCO₃. In order to achieve
18 relatively unagglomerated suspensions in this background, the 2 g/L stock was prepared by
19 slurring the TiO₂ powder in 0.15 mL of alkaline solution (1 mM NaOH) instead of DIW, then
20 continuing with the same preparation reported above, such that the NPs were not taken through
21 the isoelectric point upon being added to the NaHCO₃ solution (final pH ≈ 9). All uncoated NPs
22 (DIW or bicarbonate matrix) were then taken through the same 20 h rotation, centrifugation, and
23 phosphate washing steps, resulting in all NPs (coated and uncoated) in the same background water
24 chemistry (10 mM phosphate, pH 8) for the photoreactivity studies.
25
26
27
28
29
30
31
32
33
34
35
36
37
38
39
40
41
42
43
44
45
46

47 *Attenuated total reflectance–Fourier transform infrared (ATR-FTIR) spectroscopy*

48

49 ATR-FTIR spectroscopy was used to probe the functional groups and interactions between
50 TiO₂ and inorganic ions in the different media (DIW vs. MHW), NOM and the salts in DIW vs.
51 MHW, and the NOM adsorbing to the TiO₂ NPs in DIW vs. MHW before and after displacement
52
53
54
55
56
57
58
59
60

1
2
3 by phosphate. All measurements were collected on a Nicolet iS50 FTIR spectrometer,
4 (ThermoFisher Scientific, Waltham, MA) on a diamond/ZnSe single reflection ATR crystal (PIKE
5 Technologies, Fitchburg, WI). Spectra were collected from 4000 to 800 cm^{-1} with a resolution of
6 2 cm^{-1} and averaged over 200 scans. The NOM samples without TiO_2 were collected as
7 supernatants from centrifuged samples as prepared for the photoreaction experiments and
8 processed as described in the SI. For the TiO_2 samples, changes in the surface chemistry of the
9 TiO_2 in the presence of the various water chemistry were monitored by in situ ATR-FTIR
10 spectroscopy. First, 6 μL of TiO_2 stock suspension (2 g/L in DIW) was dried onto the ATR crystal.
11 Four separate in situ experiments were conducted to expose the TiO_2 to the different conditions:
12 (1) DIW followed by (\rightarrow) phosphate buffer (pH 8) to identify adsorbed phosphate; (2) DIW \rightarrow
13 MHW \rightarrow phosphate buffer to identify adsorbed bicarbonate and displacement by phosphate; and
14 (3) DIW \rightarrow NOM in DIW \rightarrow phosphate and (4) MHW \rightarrow NOM in MHW \rightarrow phosphate buffer to
15 evaluate NOM adsorption and displacement by phosphate. For Experiments 1 and 2, 40 μL of the
16 salt solutions were pipetted over the TiO_2 NPs, spectra were collected every 10 minutes for 30
17 minutes total, then the overlying solution was pipetted away to replace with the following solution
18 and spectra collected similarly. For Experiments 3 and 4, after taking spectra in the background
19 electrolyte as noted, 60 μL of NOM in the background solution was applied, and the NOM
20 adsorption spectra were collected every 10 minutes for 60 minutes; finally, desorption was
21 monitored after two phosphate washes with spectra collected every 10 minutes for 20 minutes in
22 each wash. To process the data, the background spectrum for subtraction was selected from a prior
23 step to evaluate the influence of each change in water chemistry.
24
25
26
27
28
29
30
31
32
33
34
35
36
37
38
39
40
41
42
43
44
45
46
47
48
49
50
51
52
53

54 *Total organic carbon (TOC) and size exclusion chromatography (SEC) analysis*
55
56
57
58
59
60

1
2
3 The adsorbed mass of NOM was evaluated by solution depletion, in which the unadsorbed
4 concentration in the supernatants from the adsorption procedure are subtracted from the initial
5 concentration to compute the adsorbed concentration. Supernatants from the two subsequent
6 phosphate washes were also collected to evaluate displacement of the NOM by the phosphate. The
7 masses of all supernatants were weighed and utilized to correct for NOM in the remaining volume
8 of supernatant from the prior wash, on the results measured in the subsequent wash.
9
10
11
12
13
14
15
16

17 Both batch TOC measurements and SEC analyses were conducted. TOC was measured on
18 a Shimadzu TOC-L analyzer with 50 μL sample injection followed by addition of sulfuric acid for
19 inorganic carbon removal, followed by oxidation of the organic carbon on a Pt catalyst at 680 $^{\circ}\text{C}$,
20 sparging with zero air, and quantification on a non-dispersive infrared detector. SEC analyses were
21 performed on an Agilent 1290 Infinity liquid chromatography (LC) system (Agilent Technologies,
22 Santa Clara, CA) equipped with a Superdex 75 10/300 GL SEC column (GE Healthcare, Chicago,
23 IL), Agilent 1260 Infinity UV-vis diode array detector, and OptiLab T-rEX differential refractive
24 index (dRI) detector (Wyatt Technologies, Santa Barbara, CA). The mobile phase was 4 mM
25 phosphate buffer (pH 7) with 25 mM NaCl^{23, 29-31} at 0.5 mL min^{-1} flowrate, the sample injection
26 volume was 100 μL , and the UV detector was set to monitor the 280 nm wavelength for aromatic
27 compounds or compounds with > 3 conjugated double bonds. The data analysis to evaluate
28 adsorption and displacement are described in the SI.
29
30
31
32
33
34
35
36
37
38
39
40
41
42
43
44
45
46

47 *Phenol photodegradation experiments*

48

49 The photocatalytic degradation of phenol was evaluated at two starting concentrations (50
50 mg/L and 20 mg/L) by the various TiO_2 NPs (0.1 g/L) in the 10 mM phosphate buffer; NP-free
51 controls were also irradiated for evaluation. Irradiation was carried out on 10 mL of sample in
52
53
54
55
56
57
58
59
60

1
2
3 quartz vials using a UV reactor (Rayonet RMR-600, Southern New England Ultraviolet Co.,
4 Branford, Connecticut) with eight fluorescent UV lamps with wavelength centered at 350 nm and
5 total irradiance of 5.0 ± 0.2 mW/cm² measured in the UVA/UVB range (UV513AB light meter,
6 GeneralTools, New York, NY), in an annular rotator with 8 vial positions and a cooling fan. In
7 every experiment, four dark (foil-wrapped) vials were placed alternately with four UV-irradiated
8 vials in the reactor as “dark controls” to evaluate any thermal degradation or other losses of phenol.
9 Samples were collected at set intervals over a total duration of 300 min. Prior to sample collection,
10 the vial was inverted three times to homogenize. The pH of all samples was measured before and
11 after the experiments. The collected samples were centrifuged at 13,000 rpm (11,337g) for 15 min
12 to pellet the NPs (Eppendorf MiniSpin Plus, Enfield, CT), and the supernatant was filtered through
13 0.22 μ m PTFE syringe filters (4 mm diameter, MicroSolv Technology, Leland, NC) to remove any
14 remnant NPs. The samples were analyzed for phenol and the degradation byproducts by LC
15 analysis as follows.
16
17
18
19
20
21
22
23
24
25
26
27
28
29
30
31
32
33
34

35 *Quantification of phenol and degradation byproducts by liquid chromatography (LC)*

36
37 All samples were quantified for phenol and its two immediate byproducts (catechol and
38 hydroquinone) by LC analysis. These byproducts were selected for quantitative analysis based on
39 their initial identification by LC–quadrupole time-of-flight (QTOF) mass spectrometry (SI Table
40 S1) and the availability of commercial material to prepare calibration standards for quantification.
41 The LC analysis was conducted on an Agilent 1260 Infinity II system equipped with an Agilent
42 Zorbax Eclipse Plus RRHD C₁₈ column (2.1 x 50 mm, 1.8 μ m). The sample injection volume was
43 5 μ L and flow rate was 0.3 mL min⁻¹. The mobile phase solvents were (A) 0.01 % acetic acid in
44 LC-MS grade water and (B) methanol, and compounds were separated using a gradient elution
45
46
47
48
49
50
51
52
53
54
55
56
57
58
59
60

1
2
3 from 95% A (5% B) to 85% A (15 % B) over 10 minutes. Subsequently, the composition was
4
5 ramped to 5% A (95% B) over 2 min and held for 3 min to flush, then ramped back to 95% A (5%
6
7 B) over 2 min and held for 6 min to re-equilibrate at the initial composition. All compounds were
8
9 quantified by the UV peak area at 272 nm as the peak wavelength for phenol.
10
11

12 *Quantification of the phenol, catechol, and hydroquinone adsorption onto the TiO₂ NPs*

14
15 The adsorption of phenol, catechol, and hydroquinone to the various phosphate-treated
16
17 TiO₂ NPs was measured to evaluate any differences in available adsorption sites for the different
18
19 surface chemistry. Because the adsorbed masses of the three compounds were low, the phosphate-
20
21 washed TiO₂ NPs were concentrated by resuspending the 15 mL of initial suspension (0.5 g/L
22
23 NPs) to only 2 mL after the last wash (3.75 g/L NPs). Then, phenol, catechol, or hydroquinone
24
25 were spiked into the NPs at 5 mg/L. Samples were allowed to rotate for 3 hours, and the supernatant
26
27 after centrifugation was filtered and analyzed by LC as above.
28
29
30
31
32

33 *Identification and evaluation of holes and ROS production*

35
36 The phosphate-treated TiO₂ were evaluated for holes or ¹O₂ generation by conducting
37
38 photodegradation experiments as above with probe compounds (KI for holes, and furfuryl alcohol
39
40 (FFA) for ¹O₂) instead of phenol. The KI assay was performed using 5 mM KI with samples
41
42 collected after 0, 15, 30, 45 and 60 min of UV exposure. The I₂ oxidation product was quantified
43
44 using the starch-iodine assay by adding 0.5 mL of sample to 0.75 mL of starch solution in a 2 mL
45
46 centrifuge tube and removing the NPs by centrifugation. The sample was stored under ice pack
47
48 and analyzed within one hour after centrifugation. 0.7 mL of supernatant was transferred to a
49
50 quartz cuvette and the absorbance at 585 nm was measured using UV-2600 spectrophotometer
51
52 (Shimadzu, Columbia, MD). The generation of singlet oxygen was analyzed by quantifying FFA
53
54
55
56
57
58
59
60

1
2
3 (15 mM initial concentration) over 60 min of UV irradiation using the same LC gradient as in the
4 phenol degradation experiment and quantifying the FFA against external calibration standards
5 using the UV signal at 230 nm.
6
7
8

9
10 All phosphate-washed NPs were prepared for EPR analysis by coating as above and
11 concentrating to 3.75 g/L by resuspending the pelleted TiO₂ NPs in a lower volume of 10 mM
12 phosphate at the end of the last wash step. Then, the TiO₂ NPs were diluted to 1 g/L in 10 mM
13 phosphate and spiked with 5 mM BMPO for EPR measurements. The samples were placed on a
14 stir plate and irradiated by top-down UV exposure using a Spectroline MiniMax lamp holder
15 (Spectronics Corp., Westbury, NY) equipped with the same 4 W UV lamp as in the phenol
16 photoreaction experiments, positioned ≈ 2.8 cm above the sample (measured irradiance of ≈ 4.67
17 mW/cm²). After 10 min exposure, samples were transferred into Kimble micro capillary pipets (50
18 μ L, DWK Lifer Sciences, Mainz, Germany) and sealed with Critoseal (Leica Microsystems,
19 Wetzlar, Germany) for EPR measurements. Room temperature EPR measurements were
20 conducted using a Bruker EMX X-band EPR spectrometer (Billerica, MA). Typical parameters
21 used were: frequency, 9.32 GHz; modulation frequency, 100 kHz; modulation amplitude, 0.1 – 0.3
22 G; microwave power, 20 mW; time constant, 327.7 ms.
23
24
25
26
27
28
29
30
31
32
33
34
35
36
37
38
39
40
41

42 **Results and Discussion**

43 *Characterization of TiO₂ NPs with NOM coatings and after phosphate treatment*

44
45 All TiO₂ stock suspensions and phosphate-treated TiO₂ NPs – either uncoated (denoted
46 “TiO₂-No NOM”) or with NOM coatings adsorbed from DIW or MHW (denoted “TiO₂-NOM_{DIW}”
47 and “TiO₂-NOM_{MHW}”, respectively) – were evaluated by DLS for their hydrodynamic size and
48 polydispersity index (PDI) (SI Figures S1a and S1b). All of the phosphate-treated NPs showed
49
50
51
52
53
54
55
56
57
58
59
60

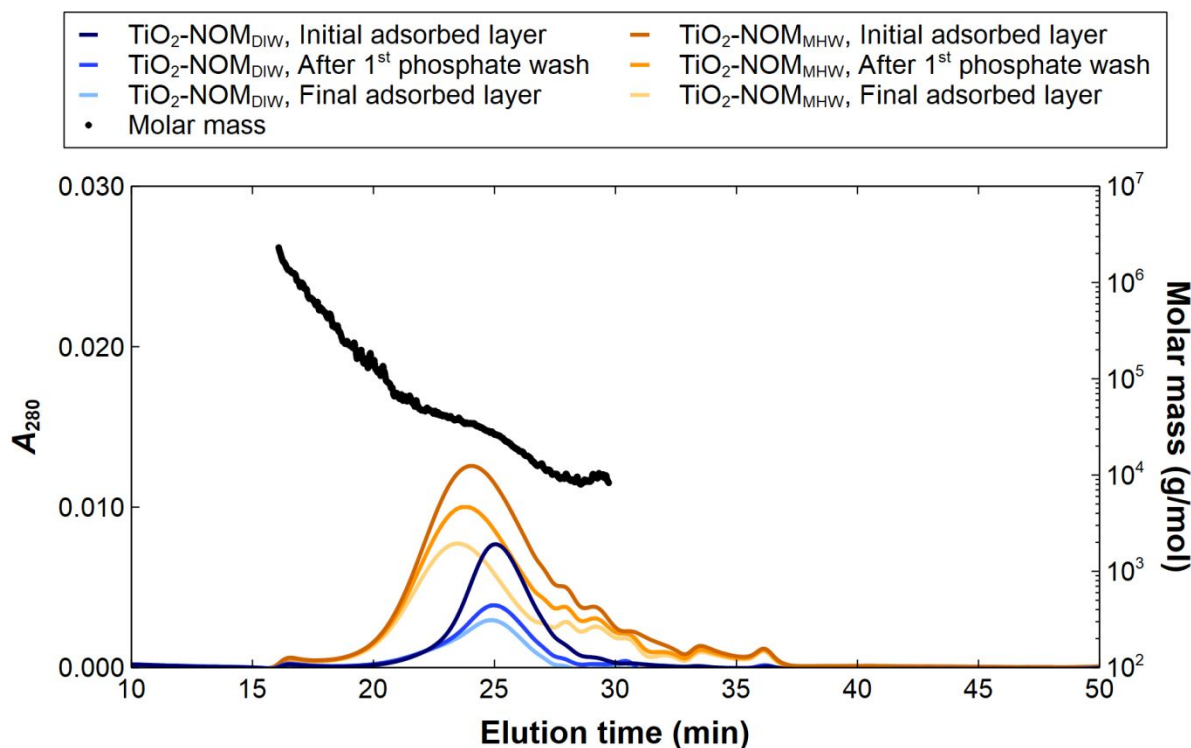
1
2
3 good redispersibility relative to the original stock suspension with mean PDI < 0.2. The zeta
4 potentials before and after phosphate washes are also provided in SI Figure S1c. The bare TiO₂ in
5 DIW (before phosphate treatment) had a positive surface charge due to acidic residues on TiO₂
6 surface from the manufacturing process,²⁶ resulting in a dispersion pH lower than the isoelectric
7 point of ≈ 7 , whereas TiO₂ NPs with NOM coating gained a negative surface charge attributable
8 to the deprotonated carboxyl groups of the adsorbed NOM. In MHW, cations (particularly Ca²⁺)
9 can provide charge screening or neutralization, resulting in a less negative charge.³² After washing
10 into 10 mM phosphate buffer, all NPs showed similarly strong negative surface charge ($\zeta < -40$
11 mV), indicative of phosphate adsorption. It is noted that bare TiO₂ NPs in MHW had ζ near zero,
12 resulting in the formation of large NP agglomerates. Thus, we did not proceed with further testing
13 of uncoated NPs in MHW for the degradation studies, as a difference in NP agglomeration state
14 could influence the generation of ROS.³³

15
16
17
18
19
20
21
22
23
24
25
26
27
28
29
30
31 ATR-FTIR was used to assess interactions between the MHW ions, NOM, and TiO₂ NPs
32 (SI Figures S2, S3, and S4). A strong phosphate peak at wavenumber $\nu = 1077 \text{ cm}^{-1}$ was observed
33 in all samples that received phosphate treatment. The possibilities for adsorption of HCO₃⁻ from
34 MHW and precipitation of calcium phosphate species when transferring from MHW to phosphate
35 buffer were also assessed. The FTIR spectra showed no observable formation of calcium
36 phosphate (hydroxyapatite) peaks³⁴ (SI Figure S2), which was also confirmed by XRD analysis
37 (SI Figure S5). Bicarbonate adsorption from MHW was observed but was then displaced upon
38 phosphate exposure (SI Figure S2). For the NOM, characteristic absorption bands representing the
39 asymmetric and symmetric stretch of the deprotonated COO⁻ groups were observed in the $\nu \approx$
40 1580 cm⁻¹ and 1400 cm⁻¹ regions, respectively, with the peak spacing between these two bands,
41 $\Delta\nu$, indicative of the binding modes.³⁵⁻³⁸ To evaluate binding mode, comparison against the
42
43
44
45
46
47
48
49
50
51
52
53
54
55
56
57
58
59
60

1
2
3 “ionic” peak spacing, $\Delta \nu_{\text{ionic}}$, is required, where $\Delta \nu_{\text{ionic}}$ was measured on NOM alone dry deposited
4 from DIW (SI Figure S3a). The NOM adsorbed to TiO_2 in DIW showed a larger peak spacing than
5
6 $\Delta \nu_{\text{ionic}}$ consistent with bidentate bridging³⁵ onto the TiO_2 surface. In MHW, a smaller peak spacing
7
8 was observed which is indicative of bidentate chelating,³⁶ however, the control NOM sample in
9
10 MHW without TiO_2 also showed similar peak spacing, suggesting the chelating is likely
11
12 attributable to NOM- Ca^{2+} interactions in solution and not necessarily the TiO_2 surface interaction.
13
14 Prior studies have similarly reported that Ca^{2+} can induce both aggregation of the deprotonated
15
16 NOM and/or bridge the negatively charged NOM to TiO_2 .^{22, 39, 40} After phosphate treatment,
17
18 significant desorption was observed for both NOM layers (SI Figure S4).
19
20
21
22
23

24 To quantify and identify the initial adsorbed species and those displaced by phosphate, the
25
26 supernatants collected from the batch samples from the initial NOM adsorption and subsequent
27
28 two washes in phosphate buffer were further analyzed. Solution depletion analysis (i.e., subtracting
29
30 the remaining from the initial NOM) of batch TOC measurements yielded initial adsorbed masses
31
32 of 50 mg/g (0.92 mg/m²) and 11 mg/g (0.20 mg/m²) in MHW and DIW, respectively. The higher
33
34 NOM adsorption in MHW is attributed to the calcium ions in MHW, which can induce bridging
35
36 of NOM to the TiO_2 surface.^{21, 22} For a more detailed analysis of which species from the NOM
37
38 mixture adsorbed initially and desorbed in the phosphate washes, SEC measurements were
39
40 performed. The raw SEC-UV-dRI chromatograms of the unadsorbed or desorbed NOM in the
41
42 supernatants are shown in SI Figure S6. The initial adsorbed NOM fraction was obtained by taking
43
44 difference chromatograms of the initial NOM and unadsorbed NOM after depletion onto the TiO_2
45
46 NPs (Figure 1). The initial NOM adsorbed in MHW and DIW was estimated to be 73 ± 4 mg/g
47
48 (1.34 ± 0.07 mg/m²) and 23 ± 4 mg/g (0.42 ± 0.08 mg/m²) respectively, based on UV detection (n
49
50 = 4 replicate experiments) (details in the SI Equation S1). The higher adsorbed mass estimate
51
52
53
54
55
56
57
58
59
60

1
2
3 compared to TOC analysis is likely attributable to adsorptive fractionation, where more aromatic
4 (UV-absorbing) species are depleted disproportionately to other species.^{23, 41} As SEC provides the
5 molecular weight distribution with larger species eluting prior to smaller compounds, Figure 1
6 further shows the adsorption of a wide range of NOM molecular weights in MHW, whereas most
7 of the adsorbed NOM in DIW was from the moderate molecular weight fraction. Although SEC-
8 dRI analysis was also conducted (SI Figure S6b), the lower signal and coelution with solvent peaks
9 precluded quantification of the total adsorbed mass.



46
47
48
49
50
51
52
53
54
55
56
57
58
59
60

Figure 1. NOM species adsorbed to the TiO_2 NPs from DIW or MHW, before and after phosphate washes, as identified by difference chromatogram analysis of SEC-UV data. The estimated molar mass of NOM across the elution time was determined by SEC with multi-angle light scattering (MALS) on a 3 g/L NOM sample (method details in the SI).

1
2
3 Desorption into the phosphate washes was evaluated directly in the supernatant of the wash
4 steps (SI Figure S6), and the remaining adsorbed NOM was computed by difference (details in the
5 SI Equation S2 and Equation S3). NOM desorption by phosphate buffer reduced the adsorbed
6 NOM concentration to 44 ± 2 mg/g (i.e., 60 ± 6 % of the initial layer remaining) and 8 ± 2 mg/g
7 (i.e., 38 ± 15 % of the initial layer remaining) in MHW and DIW, respectively ($n = 3$ replicate
8 experiments). Phosphate washes resulted in desorption of primarily the moderate molecular weight
9 fractions from both the NOM_{DIW} and the NOM_{MHW} layers (Figure 1). Overall, it can be concluded
10 that different adsorbed masses and species of NOM species were adsorbed in DIW and MHW, and
11 that these differences persisted even after partial displacement of the NOM by phosphate.
12
13
14
15
16
17
18
19
20
21
22
23
24
25

26 *Influence of remaining NOM coating layers on phenol degradation and byproduct formation*

27
28 The reactivity of the NOM-coated TiO_2 NPs is hypothesized to potentially be influenced
29 by the total adsorbed mass of NOM, as well as its composition and conformation. The
30 photocatalytic degradation and byproduct formation for 20 mg/L phenol (Figure 2) and 50 mg/L
31 phenol (Figure 3) were compared using TiO_2 -No NOM, TiO_2 - NOM_{DIW} , and TiO_2 - NOM_{MHW} in 10
32 mM phosphate buffer. It is noted that in photodegradation experiments without phosphate
33 treatment, the TiO_2 NPs without NOM agglomerate substantially over the course of the 300 min
34 photodegradation experiments (z -average hydrodynamic diameter $\gg 1$ μm by DLS) because of
35 charge neutralization or screening, either directly by Ca^{2+} in the case of the MHW background or
36 because of phenol byproduct formation (likely organic acids)⁴²⁻⁴⁶ that can adsorb and neutralize
37 the positive TiO_2 NP surface charge in DI water (below the isoelectric point of the NPs). Hence,
38 only phosphate-treated NPs are compared where no significant changes in pH or DLS size of the
39 NPs were observed after 300 min of irradiation in the phosphate buffer.
40
41
42
43
44
45
46
47
48
49
50
51
52
53
54
55
56
57
58
59
60

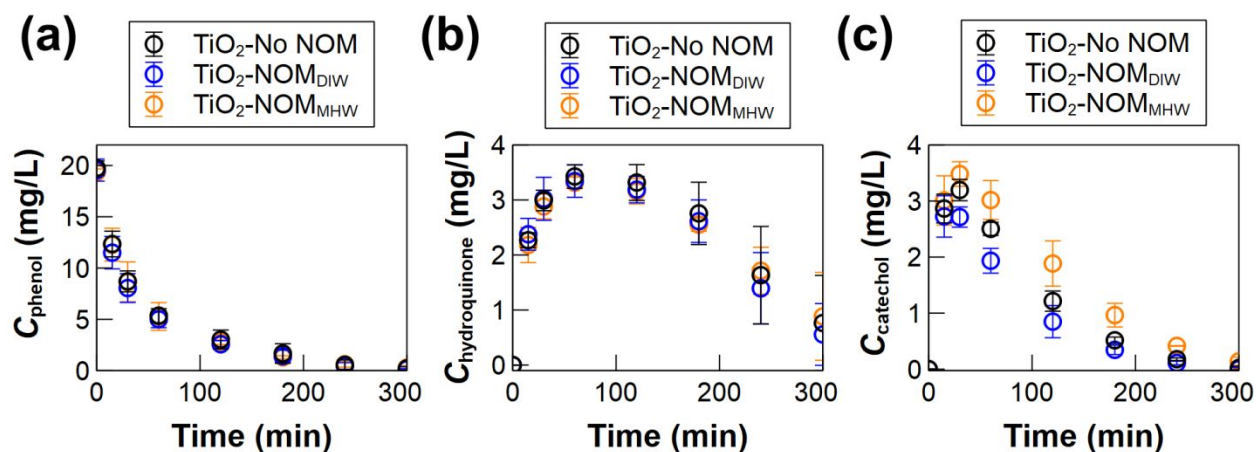


Figure 2. Degradation of 20 mg/L phenol (a), and formation and/ or degradation of hydroquinone (b) and catechol (c) using 100 mg/L of TiO₂-No NOM, TiO₂-NOM_{DIW}, or TiO₂-NOM_{MHW} (all in 10 mM phosphate buffer). No phenol losses were observed in dark controls after 300 min (not shown). Error bars represent standard deviation across triplicate experiments.

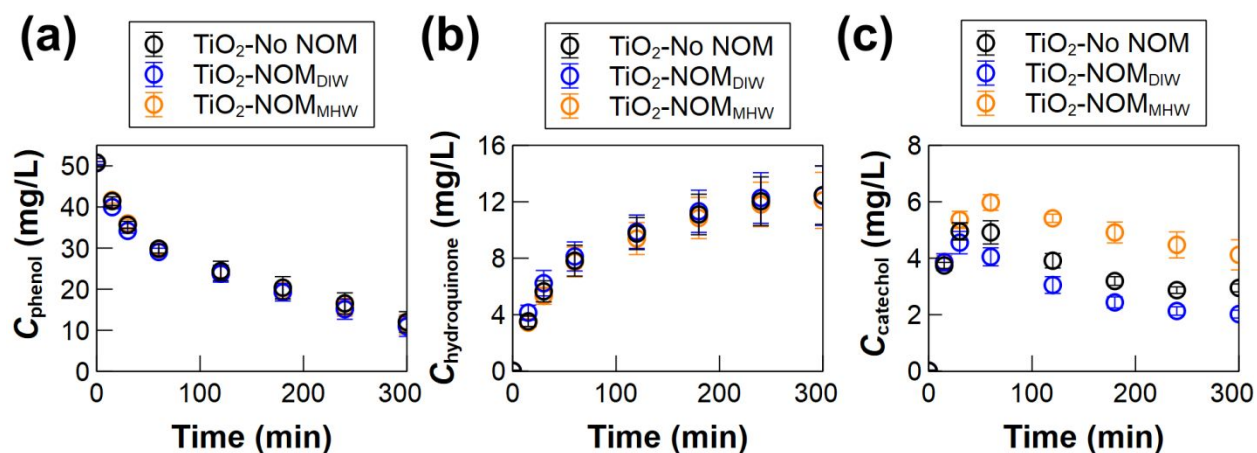


Figure 3. Degradation of 50 mg/L phenol (a), and formation and/ or degradation of hydroquinone (b) and catechol (c) using 100 mg/L of TiO₂-No NOM, TiO₂-NOM_{DIW}, or TiO₂-NOM_{MHW} (all in 10 mM phosphate buffer). No phenol losses were observed in dark controls after 300 min (not shown). Error bars represent standard deviation across triplicate experiments.

1
2
3
4
5
6 For phenol itself, no significant differences were observed in the rate of degradation
7
8 between any of the cases (Figure 2a, Figure 3a). Further investigations of the response of the two
9
10 immediate oxidation byproducts of phenol – hydroquinone and catechol – were conducted to more
11
12 comprehensively evaluate differences in reactivity. Here we focus on these early stage byproducts
13
14 that were identifiable quantifiable in the LC analysis (example chromatogram and QTOF mass
15
16 spectra in SI Figures S7a and S7b); note that further byproducts can also form as the reaction
17
18 proceeds^{24, 42-49} but could not be quantified here if external standards were not commercially
19
20 available. However, the overall mineralization efficiency was measured by TOC removal after 300
21
22 min of irradiation was less than 13 % for the different TiO₂ NPs (SI Figure S8). Considering that
23
24 the contribution of carbon from the remaining adsorbed NOM was 0.31 ± 0.07 mg C/L and $1.74 \pm$
25
26 0.09 mg C/L for TiO₂-NOM_{DIW} and TiO₂-NOM_{MHW}, respectively, compared to the added phenol
27
28 contribution of 38.3 mg C/L, the TOC is primarily from phenol and its byproducts formed in the
29
30 mineralization process. A mole balance for the three measured phenolic compounds (SI Figure S9)
31
32 accounted for < 60 % of the measured TOC at the end of the 300 min experiments, indicating that
33
34 a significant amount of other byproducts are also present in the samples. Dark controls for the NPs
35
36 with phenol and NP-free controls (irradiated mixtures of phenol, catechol, or hydroquinone and 5
37
38 mg/L of NOM) showed no significant losses of phenol and no significant production of the
39
40 byproducts of interest over the 300 min experiment.
41
42
43
44
45

46
47 Similar to phenol, there was no difference in the formation or degradation of hydroquinone
48
49 with the different NOM layers (Figure 2b, Figure 3b). On the contrary, the degradation profile of
50
51 catechol was not only distinct in the different NOM-coated TiO₂ NPs, but the two coatings induced
52
53 *opposite* effects on the reactivity: TiO₂-NOM_{DIW} showed enhanced catechol degradation, whereas
54
55
56
57
58
59
60

1
2
3 TiO₂-NOM_{MHW} showed suppressed catechol degradation (Figure 2c, Figure 3c). To explore and
4 eliminate the possible role of bicarbonate ions in the TiO₂-NOM_{MHW} samples, studies were also
5 conducted using TiO₂ NPs exposed to NaHCO₃ before phosphate treatment. Prior studies have
6 reported contradictory results on the effects of bicarbonate. Bicarbonate can enhance
7 degradation⁵⁰, e.g. via increased hole generation particularly at low concentrations,³ or by
8 scavenging electrons to enhance hole longevity, leading to overall higher hydroxyl radical
9 formation.⁵¹ However, other studies contradictorily reported that bicarbonate can scavenge holes⁵²
10 and quench hydroxyl radicals^{3, 5} to form bicarbonate radicals and thus have an inhibitory effect on
11 the TiO₂ reactivity. In the present study, the degradation of phenol, as well as the formation and/or
12 degradation of hydroquinone and catechol, using TiO₂ exposed to bicarbonate was similar to bare
13 TiO₂, suggesting that bicarbonate ions did not significantly influence the rate of degradation here
14 (SI Figure S10), which is consistent with the fact that phosphate treatment displaces the
15 bicarbonate (SI Figure S2). Hence, the key differences observed for TiO₂-NOM_{MHW} are
16 attributable to the NOM coating (not the MHW exposure).

17
18
19 Overall, the results for phenol loss are consistent with those reported by Long et al.¹⁸ that
20 phosphate can mitigate the inhibitory effect of NOM. However, the distinctive effects of the two
21 NOM layers on catechol degradation suggest that (1) catechol reacts by a different degradation
22 pathway and/or interacts differently with the adsorbed NOM than phenol or hydroquinone, and (2)
23 differences in the NOM layer properties can persist and influence the NP reactivity even after
24 phosphate treatment.

1
2
3 *Differences in catechol degradation are mediated by physical blocking and differences in ROS*
4 *speciation for NOM_{MHW} layers and enhanced hole reactivity for NOM_{DIW} layers*
5
6

7
8 We hypothesized that catechol may be undergoing specific surface reactions (as opposed
9
10 to reaction with more highly reactive ROS such as hydroxyl radical) and hence be more
11 significantly influenced by differences in the NOM surface coatings. Indeed, prior studies have
12 reported that catechol can degrade through oxidation by holes whereas phenol and hydroquinone
13 degradation are hydroxyl radical mediated.^{17, 53}
14
15
16
17
18

19 To further evaluate this hypothesis, we first studied the degradation using 20 mg/L catechol
20 alone (i.e., not as a byproduct of phenol oxidation). Unlike the catechol produced in the phenol
21 degradation experiments, no significant differences were observed for pure catechol between the
22 bare or coated TiO₂ NPs (SI Figure S11). This result could be attributable to the lack of competition
23 with phenol and other byproducts for ROS and/or surface sorption sites, and hence exacerbated
24 differences among the TiO₂ NPs with different NOM coatings in the phenol reaction experiments.
25
26 Adsorption studies of each contaminant (phenol, hydroquinone, and catechol) to the TiO₂ NPs
27 without light exposure were thus conducted to investigate potential differences in the physical
28 interaction with surface sites with the different NOM coatings. Further experiments to probe for
29 holes and various types of ROS were also performed without phenol to directly evaluate the
30 reaction modes of the TiO₂ NPs themselves, without interference from phenol or its byproducts.
31
32
33
34
35
36
37
38
39
40
41
42
43
44
45
46

47 Adsorptive interactions: It has been well-established that the adsorptive interaction is
48 critical for direct oxidation by holes¹⁷ or surface-localized ROS species. Hence, the adsorption of
49 phenol, hydroquinone, and catechol on the different TiO₂ NPs were evaluated (Figure 4).
50
51 Comparing the three compounds in general across all the bare and coated NPs, there was no
52
53
54
55
56
57
58
59
60

1
2
3 measurable adsorption of phenol, in agreement with prior studies indicating the absence of phenol
4
5 adsorption to TiO₂ surface because of a lack of stereochemical configuration that favors
6
7 adsorption.⁵⁴ Rather, catechol showed the highest degree of adsorption compared to phenol and
8
9 hydroquinone (Figure 4). These results are also in agreement with previous studies showing an
10
11 effect of the position of the hydroxylation on adsorption to TiO₂: the *ortho* hydroxyl position
12
13 (catechol) was found to favor adsorption through surface chelate coordination, while the *para*
14
15 position (hydroquinone) showed lower adsorption.^{17, 55}
16
17
18

19 Comparing the different TiO₂ surface chemistries, TiO₂-NOM_{MHW} showed the lowest
20
21 catechol and hydroquinone adsorption between the different TiO₂ NPs (with a significant
22
23 difference at > 95% confidence compared to TiO₂-No NOM, $p = 0.012$ and 0.017 for catechol and
24
25 hydroquinone, respectively), which could be attributed to the higher adsorbed mass of NOM and
26
27 hence thicker or less patchy NOM layer, resulting in more limited available surface sites for
28
29 adsorption and reaction of the catechol at the TiO₂ surface, and hence the longer persistence of
30
31 catechol for TiO₂-NOM_{MHW} in the phenol degradation studies (Figure 2c, Figure 3c). However,
32
33 no significant difference in catechol adsorption was observed between TiO₂-No NOM and TiO₂-
34
35 NOM_{DIW} ($p = 0.61$) that could explain the enhanced reactivity of TiO₂-NOM_{DIW} toward catechol.
36
37 Hence, to more fully evaluate the mechanisms influencing differences in catechol degradation
38
39 between the TiO₂ NPs, further investigations on ROS generation and hole generation were
40
41 conducted.
42
43
44
45
46
47
48
49
50
51
52
53
54
55
56
57
58
59
60

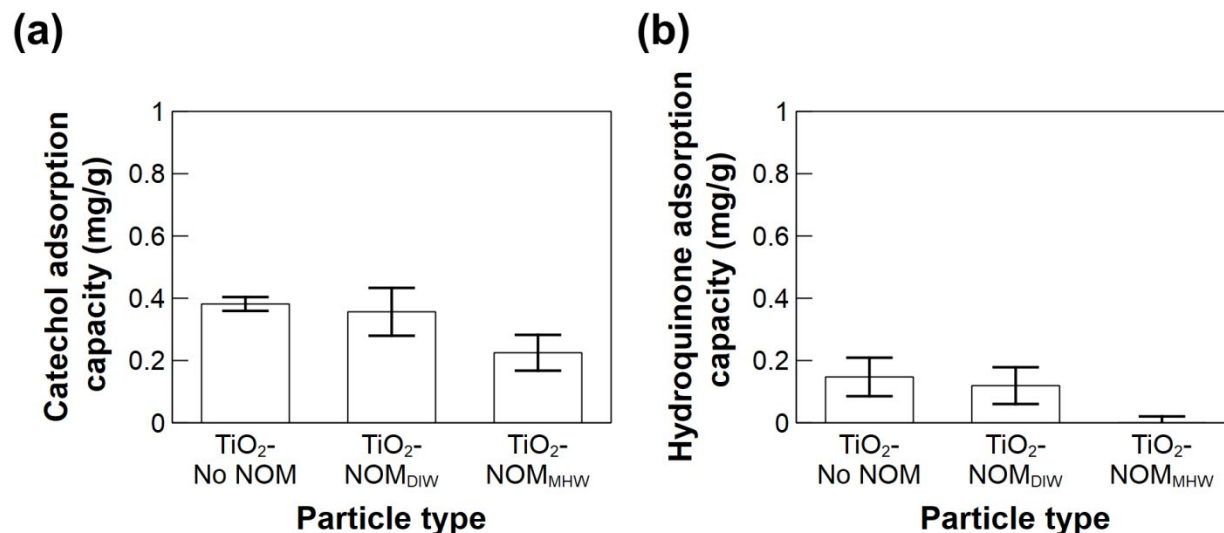
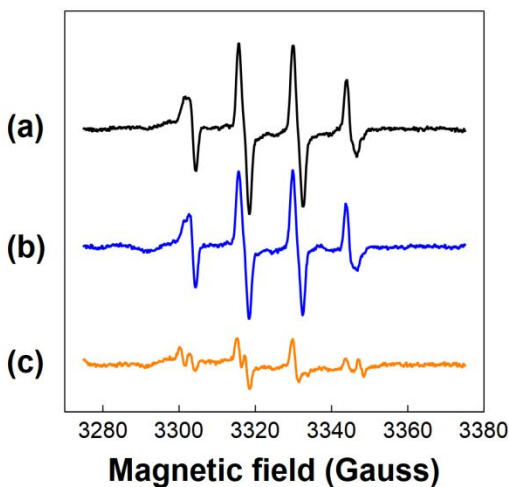


Figure 4. Adsorbed mass of catechol (a) and hydroquinone (b) onto TiO₂-No NOM, TiO₂-NOM_{DIW}, and TiO₂-NOM_{MHW} from 5 mg/L initial concentrations of the catechol and hydroquinone in 10 mM phosphate buffer. Error bars represent standard deviation across triplicate experiments.

Generation of reactive oxygen species: Singlet oxygen generation by the TiO₂-No NOM, TiO₂-NOM_{DIW} and TiO₂-NOM_{MHW} was evaluated using furfuryl alcohol as probe compound; no significant difference was observed across any of the NPs (SI Figure S12). However, distinctive results were obtained by EPR spectroscopy using BMPO to trap transient radical species^{56, 57} generated during 10 min of UV irradiation (Figure 5). In the reactions with TiO₂-No NOM and TiO₂-NOM_{DIW}, the trapped radical species were predominately hydroxyl radical (Figures 5a and 5b). The BMPO-OH adduct existed in an equilibrium of two conformers, with the same g value but slightly different hyperfine splittings (SI Figure S13), giving rise to the overall symmetric EPR lineshape (Figures 5a and 5b). On the other hand, in the reaction with TiO₂-NOM_{MHW}, the EPR lineshape of the BMPO-radical adduct(s) was asymmetric indicating that different radical species

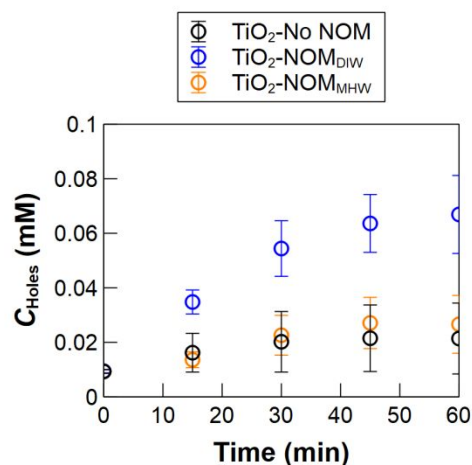
1
2
3 were trapped (Figure 5c). Significantly lower radical species were trapped in the reaction with
4
5 $\text{TiO}_2\text{-NOM}_{\text{MHW}}$ (Figure 5c). Therefore, in addition to the lower physical adsorption of catechol to
6
7 the $\text{TiO}_2\text{-NOM}_{\text{MHW}}$, different types of radical species generated at lower level may contribute to
8
9 the slower degradation of catechol by $\text{TiO}_2\text{-NOM}_{\text{MHW}}$. However, similar amounts of radical were
10
11 trapped in the reactions with $\text{TiO}_2\text{-No NOM}$ and $\text{TiO}_2\text{-NOM}_{\text{DIW}}$ (Figures 5a and 5b), and hence
12
13 the enhanced reactivity of $\text{TiO}_2\text{-NOM}_{\text{DIW}}$ could not be explained by ROS as probed here.
14
15
16
17



18
19
20
21
22
23
24
25
26
27
28
29
30
31
32
33
34
35 **Figure 5.** EPR spectra of BMPO-radical adduct(s) formed in the UV irradiation reactions with
36
37 $\text{TiO}_2\text{-No NOM}$ (a); $\text{TiO}_2\text{-NOM}_{\text{DIW}}$ (b); and $\text{TiO}_2\text{-NOM}_{\text{MHW}}$ (c).
38
39
40

41
42 Hole generation: Holes can induce the oxidation of pollutants by direct electron transfer at
43
44 the NP surface.¹⁷ The holes were quantified by a starch-iodine assay to quantify iodine produced
45
46 from the reaction of 5 mM KI. Notably, $\text{TiO}_2\text{-NOM}_{\text{DIW}}$ showed enhanced hole generation
47
48 compared to $\text{TiO}_2\text{-No NOM}$ and $\text{TiO}_2\text{-NOM}_{\text{MHW}}$ (Figure 6). Prior studies reported that positively
49
50 charged NOM radicals can be produced by electron transfer between electron donating and
51
52 accepting moieties within NOM or photoionization of NOM that results in loss of electrons^{14, 15}
53
54 and hence act as additional holes. Therefore, an enhancement in direct hole oxidation of catechol
55
56
57
58
59
60

1
2
3 can explain the increased catechol degradation using $\text{TiO}_2\text{-NOM}_{\text{DIW}}$. However, no increase or
4
5 decrease in hole generation was observed in $\text{TiO}_2\text{-NOM}_{\text{MHW}}$ relative to $\text{TiO}_2\text{-No NOM}$. Because
6
7 the $\text{TiO}_2\text{-NOM}_{\text{MHW}}$ coating was comprised of high and low molecular weight species, in addition
8
9 to the moderate molecular weight species observed in NOM_{DIW} , it is possible that either the
10
11 specific conformation of the NOM_{MHW} layer is not conducive to enhanced electron transfer, or any
12
13 enhanced formation of holes or positively-charged radicals is countered by scavenging from the
14
15 additional NOM species adsorbed in $\text{TiO}_2\text{-NOM}_{\text{MHW}}$.
16
17
18
19
20



21
22
23
24
25
26
27
28
29
30
31
32
33
34
35
36
37 **Figure 6.** Quantification of holes generated upon irradiation of the TiO_2 NPs in 10 mM phosphate.
38
39 Error bars represent standard deviation across four replicate experiments.
40
41
42
43

44 **Conclusions and Implications**

45
46 This study identified that the detailed properties of adsorbed NOM coatings, including
47
48 differences in adsorptive fractionation from a single type of NOM (e.g., Suwannee River NOM)
49
50 in different water chemistry (DIW and MHW), can have persistent influences on the reactivity of
51
52 TiO_2 NPs even after partial displacement of the NOM by phosphate. Although phenol degradation
53
54 was not impacted by the residual NOM after phosphate treatment of the bare or NOM-coated
55
56
57
58
59
60

1
2
3 particles, the degradation of its catechol byproduct was either enhanced or suppressed, depending
4
5 on the NOM adsorption condition. These findings imply that evaluation of only a single “model”
6
7 probe compound such as phenol may preclude a full understanding of the photocatalytic reactivity,
8
9 whereas byproduct analysis provides additional insights into a wider range of reaction pathways.
10
11 Furthermore, this study demonstrated that a mechanistic explanation for differences in the
12
13 photoreactivity of NOM-coated nanoparticles required consideration of not only the ROS species
14
15 generated, but also direct surface interactions with the NPs, both physical adsorption of catechol,
16
17 and direct electron transfer interactions such as hole formation. These considerations can be
18
19 important in the application of photoreactive nanoparticles, as the overall hazard profile of the
20
21 treated water will require an understanding not only of the removal of the original pollutants but
22
23 also the types and persistence of byproducts formed.
24
25
26
27
28
29

30 **Acknowledgements**

31
32 We gratefully acknowledge Dr. Michael Harold for FTIR instrument access, Dr. Vincent A.
33
34 Hackley for the NIST SRM 1898 TiO₂ NPs, Dr. Gregory V. Lowry for the SEC column, and Dr.
35
36 Charisma Lattao for general lab assistance. We also acknowledge the National Science Foundation
37
38 (NSF) CBET 1705511 for funding.
39
40
41
42
43

44 **Electronic Supplementary Information**

45
46 Additional NP characterization (DLS, polydispersity index and zeta potential measurements),
47
48 XRD and ATR-FTIR spectra, SEC chromatograms and method information, LC-QTOF methods
49
50 and data, and probe reactivity experiments.
51
52
53
54
55
56
57

References

1. D. Friedmann, C. Mendive and D. Bahnemann, TiO₂ for water treatment: Parameters affecting the kinetics and mechanisms of photocatalysis, *Appl. Catal., B*, 2010, **99**, 398-406.
2. D. Awfa, M. Ateia, M. Fujii and C. Yoshimura, Novel Magnetic Carbon Nanotube-TiO₂ Composites for Solar Light Photocatalytic Degradation of Pharmaceuticals in the Presence of Natural Organic Matter, *J. Water Process Eng.*, 2019, **31**, 100836.
3. J. Farner Budarz, A. Turolla, A. F. Piasecki, J.-Y. Bottero, M. Antonelli and M. R. Wiesner, Influence of Aqueous Inorganic Anions on the Reactivity of Nanoparticles in TiO₂ Photocatalysis, *Langmuir*, 2017, **33**, 2770-2779.
4. T. Makropoulou, I. Kortidis, K. Davididou, D. E. Motaung and E. Chatzisyneon, Photocatalytic facile ZnO nanostructures for the elimination of the antibiotic sulfamethoxazole in water, *J. Water Process Eng.*, 2020, **36**, 101299.
5. R. Yuan, Y. Zhu, B. Zhou and J. Hu, Photocatalytic oxidation of sulfamethoxazole in the presence of TiO₂: Effect of matrix in aqueous solution on decomposition mechanisms, *Chem. Eng. J.*, 2019, **359**, 1527-1536.
6. Y.-M. Kang, M.-K. Kim and K.-D. Zoh, Effect of nitrate, carbonate/bicarbonate, humic acid, and H₂O₂ on the kinetics and degradation mechanism of Bisphenol-A during UV photolysis, *Chemosphere*, 2018, **204**, 148-155.
7. D. Awfa, M. Ateia, M. Fujii and C. Yoshimura, Photocatalytic degradation of organic micropollutants: Inhibition mechanisms by different fractions of natural organic matter, *Water Res.*, 2020, **174**, 115643.

- 1
2
3 8. L. Gao, B. Zhou, F. Wang, R. Yuan, H. Chen and X. Han, Effect of dissolved organic
4 matters and inorganic ions on TiO₂ photocatalysis of diclofenac: mechanistic study and
5 degradation pathways, *Environ. Sci. Pollut. Res. Int.*, 2020, **27**, 2044-2053.
6
7
- 8
9
10 9. L. Hu, P. M. Flanders, P. L. Miller and T. J. Strathmann, Oxidation of sulfamethoxazole
11 and related antimicrobial agents by TiO₂ photocatalysis, *Water Res.*, 2007, **41**, 2612-
12 2626.
13
14
- 15
16
17 10. J. Brame, M. Long, Q. Li and P. Alvarez, Inhibitory effect of natural organic matter or
18 other background constituents on photocatalytic advanced oxidation processes:
19 Mechanistic model development and validation, *Water Res.*, 2015, **84**, 362-371.
20
21
- 22
23
24 11. H. Wu, L. Huang, A. Rose and V. H. Grassian, Impact of surface adsorbed biologically
25 and environmentally relevant coatings on TiO₂ nanoparticle reactivity, *Environ. Sci.:*
26 *Nano*, 2020, **7**, 3783-3793.
27
28
- 29
30
31 12. J. M. Farner, R. S. Cheong, E. Mahé, H. Anand and N. Tufenkji, Comparing TiO₂
32 nanoparticle formulations: stability and photoreactivity are key factors in acute toxicity to
33 *Daphnia magna*, *Environ. Sci.: Nano*, 2019, **6**, 2532-2543.
34
35
- 36
37
38 13. S. Garg, A. L. Rose and T. D. Waite, Photochemical production of superoxide and
39 hydrogen peroxide from natural organic matter, *Geochim. Cosmochim. Acta*, 2011, **75**,
40 4310-4320.
41
42
- 43
44
45 14. Y. Li, Y. Pan, L. Lian, S. Yan, W. Song and X. Yang, Photosensitized degradation of
46 acetaminophen in natural organic matter solutions: The role of triplet states and oxygen,
47 *Water Res.*, 2017, **109**, 266-273.
48
49
50
51
52
53
54
55
56
57

- 1
2
3 15. Y. Zhang, R. Del Vecchio and N. V. Blough, Investigating the Mechanism of Hydrogen
4 Peroxide Photoproduction by Humic Substances, *Environ. Sci. Technol.*, 2012, **46**,
5 11836-11843.
6
7
- 8
9
10 16. C. S. Uyguner-Demirel, N. C. Birben and M. Bekbolet, Elucidation of background
11 organic matter matrix effect on photocatalytic treatment of contaminants using TiO₂: A
12 review, *Catal. Today*, 2017, **284**, 202-214.
13
14
- 15
16
17 17. D. Zhao, C. Chen, Y. Wang, H. Ji, W. Ma, L. Zang and J. Zhao, Surface Modification of
18 TiO₂ by Phosphate: Effect on Photocatalytic Activity and Mechanism Implication, *J.*
19 *Phys. Chem. C*, 2008, **112**, 5993-6001.
20
21
- 22
23
24 18. M. Long, J. Brame, F. Qin, J. Bao, Q. Li and P. J. J. Alvarez, Phosphate Changes Effect
25 of Humic Acids on TiO₂ Photocatalysis: From Inhibition to Mitigation of Electron–Hole
26 Recombination, *Environ. Sci. Technol.*, 2017, **51**, 514-521.
27
28
- 29
30
31 19. M. Erhayem and M. Sohn, Stability studies for titanium dioxide nanoparticles upon
32 adsorption of Suwannee River humic and fulvic acids and natural organic matter, *Sci.*
33 *Total Environ.*, 2014, **468-469**, 249-257.
34
35
- 36
37
38 20. I. Sit, H. Wu and V. H. Grassian, Environmental Aspects of Oxide Nanoparticles:
39 Probing Oxide Nanoparticle Surface Processes Under Different Environmental
40 Conditions, *Annu. Rev. Anal. Chem.*, 2021, DOI: 10.1146/annurev-anchem-091420-
41 092928.
42
43
- 44
45
46
47 21. J. E. Kilduff, T. Karanfil and W. J. Weber, Competitive Interactions among Components
48 of Humic Acids in Granular Activated Carbon Adsorption Systems: Effects of Solution
49 Chemistry, *Environ. Sci. Technol.*, 1996, **30**, 1344-1351.
50
51
52
53
54
55
56
57
58
59
60

- 1
2
3 22. M. Luo, Y. Huang, M. Zhu, Y.-n. Tang, T. Ren, J. Ren, H. Wang and F. Li, Properties of
4 different natural organic matter influence the adsorption and aggregation behavior of
5
6 TiO₂ nanoparticles, *J. Saudi Chem. Soc.*, 2018, **22**, 146-154.
7
8
9
10 23. S. Shakiba, A. Hakimian, L. R. Barco and S. M. Louie, Dynamic Intermolecular
11 Interactions Control Adsorption from Mixtures of Natural Organic Matter and Protein
12 onto Titanium Dioxide Nanoparticles, *Environ. Sci. Technol.*, 2018, **52**, 14158-14168.
13
14
15
16 24. D. Vione, T. Picatonotto and M. E. Carlotti, Photodegradation of phenol and salicylic
17 acid by coated rutile-based pigments: a new approach for the assessment of sunscreen
18 treatment efficiency, *J. Cosmet. Sci.*, 2003, **54**, 513-524.
19
20
21
22
23 25. K. Lv, X. Guo, X. Wu, Q. Li, W. Ho, M. Li, H. Ye and D. Du, Photocatalytic selective
24 oxidation of phenol to produce dihydroxybenzenes in a TiO₂/UV system: Hydroxyl
25 radical versus hole, *Appl. Catal., B*, 2016, **199**, 405-411.
26
27
28
29
30 26. National Institute of Standards and Technology (NIST). *Certificate of Analysis: SRM*
31 *1898 - Titanium dioxide nanomaterials*, Gaithersburg, MD, 2020.
32
33
34
35 27. S. Li and J. Hu, Transformation products formation of ciprofloxacin in UVA/LED and
36 UVA/LED/TiO₂ systems: Impact of natural organic matter characteristics, *Water Res.*,
37 2018, **132**, 320-330.
38
39
40
41
42 28. X. Cheng, H. Guo, Y. Zhang, X. Wu and Y. Liu, Non-photochemical production of
43 singlet oxygen via activation of persulfate by carbon nanotubes, *Water Res.*, 2017, **113**,
44 80-88.
45
46
47
48
49 29. S. M. Louie, R. D. Tilton and G. V. Lowry, Effects of Molecular Weight Distribution and
50 Chemical Properties of Natural Organic Matter on Gold Nanoparticle Aggregation,
51 *Environ. Sci. Technol.*, 2013, **47**, 4245-4254.
52
53
54
55
56
57
58
59
60

- 1
2
3 30. Z. Li, S. Shakiba, N. Deng, J. Chen, S. M. Louie and Y. Hu, Natural Organic Matter
4 (NOM) Imparts Molecular-Weight-Dependent Steric Stabilization or Electrostatic
5 Destabilization to Ferrihydrite Nanoparticles, *Environ. Sci. Technol.*, 2020, **54**, 6761-
6 6770.
7
8
9
10
11
12 31. S. M. Louie, E. R. Spielman-Sun, M. J. Small, R. D. Tilton and G. V. Lowry, Correlation
13 of the Physicochemical Properties of Natural Organic Matter Samples from Different
14 Sources to Their Effects on Gold Nanoparticle Aggregation in Monovalent Electrolyte,
15 *Environ. Sci. Technol.*, 2015, **49**, 2188-2198.
16
17
18
19
20
21 32. H. Zhang, W. Wang, H. Zhao, L. Zhao, L.-Y. Gan and L.-H. Guo, Facet-mediated
22 interaction between humic acid and TiO₂ nanoparticles: implications for aggregation and
23 stability kinetics in aquatic environments, *Environ. Sci.: Nano*, 2019, **6**, 1754-1764.
24
25
26
27
28 33. D. Jassby, J. Farner Budarz and M. Wiesner, Impact of Aggregate Size and Structure on
29 the Photocatalytic Properties of TiO₂ and ZnO Nanoparticles, *Environ. Sci. Technol.*,
30 2012, **46**, 6934-6941.
31
32
33
34
35 34. E. Ahounbar, S. M. Mousavi Khoei and H. Omidvar, Characteristics of in-situ
36 synthesized Hydroxyapatite on TiO₂ ceramic via plasma electrolytic oxidation, *Ceram.*
37 *Int.*, 2019, **45**, 3118-3125.
38
39
40
41
42 35. S. Jayalath, H. Wu, S. C. Larsen and V. H. Grassian, Surface Adsorption of Suwannee
43 River Humic Acid on TiO₂ Nanoparticles: A Study of pH and Particle Size, *Langmuir*,
44 2018, **34**, 3136-3145.
45
46
47
48
49 36. G. B. Deacon and R. J. Phillips, Relationships between the carbon-oxygen stretching
50 frequencies of carboxylato complexes and the type of carboxylate coordination, *Coord.*
51 *Chem. Rev.*, 1980, **33**, 227-250.
52
53
54
55
56
57
58
59
60

- 1
2
3 37. H. Wu, N. I. Gonzalez-Pech and V. H. Grassian, Displacement reactions between
4 environmentally and biologically relevant ligands on TiO₂ nanoparticles: insights into the
5 aging of nanoparticles in the environment, *Environ. Sci.: Nano*, 2019, **6**, 489-504.
6
7
8
9
10 38. C. C. R. Sutton, G. da Silva and G. V. Franks, Modeling the IR Spectra of Aqueous
11 Metal Carboxylate Complexes: Correlation between Bonding Geometry and Stretching
12 Mode Wavenumber Shifts, *Chem. Eur. J.*, 2015, **21**, 6801-6805.
13
14
15
16
17 39. J. Kim, W. Shan, S. H. R. Davies, M. J. Baumann, S. J. Masten and V. V. Tarabara,
18 Interactions of Aqueous NOM with Nanoscale TiO₂: Implications for Ceramic Membrane
19 Filtration-Ozonation Hybrid Process, *Environ. Sci. Technol.*, 2009, **43**, 5488-5494.
20
21
22
23
24 40. X. Z. Li, C. M. Fan and Y. P. Sun, Enhancement of photocatalytic oxidation of humic
25 acid in TiO₂ suspensions by increasing cation strength, *Chemosphere*, 2002, **48**, 453-460.
26
27
28
29 41. G. V. Korshin, C.-W. Li and M. M. Benjamin, Monitoring the properties of natural
30 organic matter through UV spectroscopy: A consistent theory, *Water Res.*, 1997, **31**,
31 1787-1795.
32
33
34
35 42. Z. Guo, R. Ma and G. Li, Degradation of phenol by nanomaterial TiO₂ in wastewater,
36 *Chem. Eng. J.*, 2006, **119**, 55-59.
37
38
39
40 43. K.-i. Okamoto, Y. Yamamoto, H. Tanaka, M. Tanaka and A. Itaya, Heterogeneous
41 Photocatalytic Decomposition of Phenol over TiO₂ Powder, *Bull. Chem. Soc. Jpn.*, 1985,
42 **58**, 2015-2022.
43
44
45
46
47 44. J. Chen, L. Eberlein and C. H. Langford, Pathways of phenol and benzene photooxidation
48 using TiO₂ supported on a zeolite, *J. Photochem. Photobiol., A*, 2002, **148**, 183-189.
49
50
51
52
53
54
55
56
57
58
59
60

- 1
2
3 45. P. Górska, A. Zaleska and J. Hupka, Photodegradation of phenol by UV/TiO₂ and
4
5 Vis/N,C-TiO₂ processes: Comparative mechanistic and kinetic studies, *Sep. Purif.*
6
7 *Technol.*, 2009, **68**, 90-96.
8
9
10 46. T. T. T. Dang, S. T. T. Le, D. Channei, W. Khanitchaidecha and A. Nakaruk,
11
12 Photodegradation mechanisms of phenol in the photocatalytic process, *Res. Chem.*
13
14 *Intermed.*, 2016, **42**, 5961-5974.
15
16
17 47. A. M. Peiró, J. A. Ayllón, J. Peral and X. Doménech, TiO₂-photocatalyzed degradation of
18
19 phenol and ortho-substituted phenolic compounds, *Appl. Catal., B*, 2001, **30**, 359-373.
20
21
22 48. A. Sobczykński, Ł. Duczmal and W. Zmudziński, Phenol destruction by photocatalysis on
23
24 TiO₂: an attempt to solve the reaction mechanism, *J. Mol. Catal. A: Chem.*, 2004, **213**,
25
26 225-230.
27
28
29 49. I. Ilisz and A. Dombi, Investigation of the photodecomposition of phenol in near-UV-
30
31 irradiated aqueous TiO₂ suspensions. II. Effect of charge-trapping species on product
32
33 distribution, *Appl. Catal., A*, 1999, **180**, 35-45.
34
35
36 50. W. W.-P. Lai, M.-H. Hsu and A. Y.-C. Lin, The role of bicarbonate anions in
37
38 methotrexate degradation via UV/TiO₂: Mechanisms, reactivity and increased toxicity,
39
40 *Water Res.*, 2017, **112**, 157-166.
41
42
43 51. A. Molinari, L. Samiolo and R. Amadelli, EPR spin trapping evidence of radical
44
45 intermediates in the photo-reduction of bicarbonate/CO₂ in TiO₂ aqueous suspensions,
46
47 *Photochem. Photobiol. Sci.*, 2015, **14**, 1039-1046.
48
49
50 52. D. E. Santiago, J. Araña, O. González-Díaz, M. E. Alemán-Dominguez, A. C. Acosta-
51
52 Dacal, C. Fernandez-Rodríguez, J. Pérez-Peña and J. M. Doña-Rodríguez, Effect of
53
54
55
56
57
58
59
60

- 1
2
3 inorganic ions on the photocatalytic treatment of agro-industrial wastewaters containing
4 imazalil, *Appl. Catal., B*, 2014, **156-157**, 284-292.
- 5
6
7
8 53. X. Li, J. W. Cubbage, T. A. Tetzlaff and W. S. Jenks, Photocatalytic Degradation of 4-
9 Chlorophenol. 1. The Hydroquinone Pathway, *J. Org. Chem.*, 1999, **64**, 8509-8524.
- 10
11
12 54. S. Tunesi and M. Anderson, Influence of chemisorption on the photodecomposition of
13 salicylic acid and related compounds using suspended titania ceramic membranes, *J.*
14 *Phys. Chem.*, 1991, **95**, 3399-3405.
- 15
16
17
18
19 55. D. Vasudevan and A. T. Stone, Adsorption of Catechols, 2-Aminophenols, and 1,2-
20 Phenylenediamines at the Metal (Hydr)Oxide/Water Interface: Effect of Ring
21 Substituents on the Adsorption onto TiO₂, *Environ. Sci. Technol.*, 1996, **30**, 1604-1613.
- 22
23
24
25
26 56. N. Khan, C. M. Wilmot, G. M. Rosen, E. Demidenko, J. Sun, J. Joseph, J. O'Hara, B.
27 Kalyanaraman and H. M. Swartz, Spin traps: in vitro toxicity and stability of radical
28 adducts, *Free Radical Biol. Med.*, 2003, **34**, 1473-1481.
- 29
30
31
32
33 57. H. Zhao, J. Joseph, H. Zhang, H. Karoui and B. Kalyanaraman, Synthesis and
34 biochemical applications of a solid cyclic nitron spin trap: a relatively superior trap for
35 detecting superoxide anions and glutathiy radicals, *Free Radical Biol. Med.*, 2001, **31**,
36 599-606.
37
38
39
40
41
42
43
44
45
46
47
48
49
50
51
52
53
54
55
56
57
58
59
60